Liquid Crystals
Publication details, including instructions for authors and subscription information:
http://www.informaworld.com/smpp/title~content=t713926090

Investigations of phase transitions in liquid crystals by means of adiabatic scanning calorimetry

Jan Thoen[a]; George Cordoyiannis[a]; Christ Glorieux[a]
[a] Laboratorium voor Akoestiek en Thermische Fysica, Departement Natuurkunde en Sterrenkunde, Katholieke Universiteit Leuven, Leuven, Belgium

To cite this Article Thoen, Jan , Cordoyiannis, George and Glorieux, Christ(2009) 'Investigations of phase transitions in liquid crystals by means of adiabatic scanning calorimetry', Liquid Crystals, 36: 6, 669 — 684
To link to this Article: DOI: 10.1080/02678290902755564
URL: http://dx.doi.org/10.1080/02678290902755564

Liquid Crystals,
Vol. 36, Nos. 6–7, June–July 2009, 669–684

Taylor & Francis
Taylor & Francis Group

INVITED ARTICLE

Investigations of phase transitions in liquid crystals by means of adiabatic scanning calorimetry

Jan Thoen*, George Cordoyiannis and Christ Glorieux

Laboratorium voor Akoestiek en Thermische Fysica, Departement Natuurkunde en Sterrenkunde, Katholieke Universiteit Leuven, Celestijnenlaan 200D, B-3001 Leuven, Belgium

(Received 19 December 2008; accepted 16 January 2009)

High-resolution calorimetric techniques have substantially contributed in characterising and understanding the delicate thermal behaviour near many phase transitions in liquid crystals. In this paper we describe a high-resolution adiabatic scanning calorimetric technique that has proven to be an important tool in discriminating between first-order and second-order phase transitions in addition to rendering high-resolution information on fluctuations-induced pretransitional specific heat capacity behaviour. The capabilities of adiabatic scanning calorimetry are illustrated with experimental results for the isotropic to nematic and the isotropic to smectic A transitions for a series of alkylcyanobiphenyl compounds. For the nematic to smectic A transition results are presented for pure compounds and mixtures of liquid crystals as well as on the effects of added non-mesogenic solutes and nanoparticles. For chiral molecules results for phase transitions involving blue phases and twist grain boundary phases are considered.

Keywords: liquid crystals; calorimetry; phase transitions; latent heat; critical behavior

1. Introduction

Liquid crystal compounds can exhibit a wide variety of stable mesophases with symmetry intermediate between that of isotropic liquids and solid crystals. Such mesophases possess orientational order but reduced or no positional order (*1–3*). The many different phases and phase transitions make liquid crystals excellent model systems for testing general phase transition and critical phenomena concepts. The first-order or second-order (or continuous) character of the transition and the universality class of the critical exponents have been investigated extensively. High-resolution adiabatic and ac calorimetric techniques have contributed substantially by revealing subtle thermal features and fluctuation effects at the phase transitions (*4–6*). In particular, adiabatic scanning calorimetry has proven to be an important tool to discriminate between first-order and second-order transitions in addition to rendering high-resolution information on pretransitional specific heat capacity behaviour (*7*).

In this (mainly review) paper, we will concentrate on results obtained by means of adiabatic scanning calorimetry (ASC) for several types of phase transitions. After presenting some general aspects of thermal behaviour of phase transitions, the specific possibilities of ASC will be explained. The subsequently discussed phase transitions and results presented will focus on (1) the isotropic to liquid crystalline phases, (2) the nematic to smectic A transition and (3) phase transitions involving blue phases and twist grain boundary phases.

2. Classification of phase transitions

Phase transitions are usually classified in first-order transitions and so-called second order or continuous ones. First-order phase transitions are thermodynamically characterised by finite discontinuities in one or more first derivatives of the relevant thermodynamic potential. For the Gibbs free energy $G(p,T)$ (appropriate for fluids) as a function of pressure p and temperature T, this means that the entropy $S = -(\partial G/\partial T)_p$ and/or the specific volume $V = (\partial G/\partial p)_T$ are discontinuous (*8,9*). At second-order (or continuous) phase transitions S and V are continuous. Thus, in order to assess whether a transition is first order or continuous, one has to verify the presence or absence, at the transition, of a discontinuity in the specific volume ΔV or in the entropy ΔS, or more conveniently, in the enthalpy, by determining the latent heat given by $\Delta H_L = T_t \Delta S$, with T_t the transition temperature. Experimentally, this is often not a simple task for first-order phase transitions with (very) small discontinuities, and requires very high-resolution density or enthalpy measurements. According to the classical Ehrenfest scheme (*10*) second-order transitions are characterised by finite discontinuities in the second derivatives of the Gibbs free energy. Thus, for second-order transitions finite discontinuities are expected for the specific heat capacity $C_p = -T(\partial S/\partial T)_p = (\partial H/\partial T)_p$, the isobaric thermal expansion coefficient $\alpha_p = V^{-1}(\partial V/\partial T)_p$, and the isothermal compressibility $\kappa_T = -V^{-1}(\partial V/\partial p)_T$. The

*Corresponding author. Email: Jan.Thoen@fys.kuleuven.be

ISSN 0267-8292 print/ISSN 1366-5855 online

DOI: 10.1080/02678290902755564
http://www.informaworld.com

Ehrenfest scheme may be extended indefinitely to even higher order transitions; however, these have never been observed. Moreover, even for so-called second-order transitions, where the first derivatives of the thermodynamic potentials remain continuous, the scheme is not useful in practice. Rather than observing discontinuities in the second derivatives of the Gibbs free energy, equal values or simultaneous divergences from both sides of the transition are observed. In this perspective it would probably be more appropriate to use the term 'continuous' transitions rather than second order. For continuous transitions quite often one uses the term 'critical point', which is only appropriate if one considers the variation of only a single thermodynamic parameter. A dominant characteristic of continuous transitions is the large increase in the microscopic fluctuations in the vicinity, which heralds the approaching transition.

In the left part of Figure 1, characteristic behaviour for the enthalpy H as a function of temperature near a transition temperature T_{tr} is shown schematically for first-order as well as for second-order transitions. The right-hand part of the figure gives the corresponding temperature behaviour of the specific heat capacity $C_p = (\partial H/\partial T)_p$.

In Figure 1(a) the temperature dependence of H near a strongly first-order transition with a large latent heat ΔH_L at T_{tr} is given. H has a nearly linear dependence on temperature below and above the transition. This results in an almost constant C_p in both phases. Figure 1(b) represents the case of a weakly first-order transition with only a small latent heat, but H shows substantial pretransitional temperature variation in both phases, which results in anomalous pretransitional increases in C_p. The total enthalpy change of the transition can be written as:

$$\Delta H_L + \delta H = \Delta H_L + \int \Delta C_p dT, \qquad (1)$$

with $\Delta C_p = C_p - C_p^b$ the excess specific heat above the background C_p^b.

Figures 1(c) to 1(e) represent three cases for second-order phase transitions. At a second-order phase transition the latent heat is zero and the specific heat capacity exhibits singular behaviour at the critical point (CP). Figure 1(c) is the case of the theoretical mean-field second-order transition with a normal linear behaviour above $T_c = T_{tr}$ and a rapid variation of the enthalpy below T_c due to the changes in the long-range order with temperature. This is reflected in a rapid change of C_p below T_c on approaching the critical point, and a discontinuous jump at T_c. The cases given in Figure 1(d) and 1(e) are critical-fluctuations-dominated continuous phase transitions with pretransitional enthalpy variations and specific heat capacity anomalies above and below T_c. The main difference between these cases is the difference in the slope of the enthalpy curve at CP, resulting in a divergence of C_p to infinity in Figure 1(d), or in a large, but finite, C_p value at T_c in Figure 1(e). The enthalpy change with the transitions is indicated by δH in the figures.

All these types of phase transitions have been encountered in the large amount of high-quality calorimetric studies during the last three decades (*4–6*). Further on we will concentrate on results obtained by means of adiabatic scanning calorimetry.

3. Adiabatic scanning calorimetry

3.1 Modes of operation of an ASC

During nearly a hundred years several different calorimetric techniques with varying degrees of accuracy and precision have been developed. Traditionally, heat capacity measurements are carried out by means of the adiabatic heat pulse method introduced by Nernst (*11*). In the experiment a known amount of heat ΔQ is (electrically) applied to the sample and the corresponding temperature rise ΔT is measured. This ΔT step has of course to be sufficiently small compared with the curvature of the enthalpy curve $H(T)$ at a given (average) temperature T, especially near a phase transition, which makes the method somewhat tedious and slow. The heat capacity (at constant pressure) of a sample at a given temperature is then obtained from:

$$C_p = \frac{\Delta Q}{\Delta T}. \qquad (2)$$

Since in this way one looks at the derivative of the enthalpy curve it should be clear that no information can be obtained on the latent heat (and thus on the order of a phase transition). Rewriting Equation (2) in the following way:

$$C_p = \frac{dQ}{dT} = \frac{dQ/dt}{dT/dt} = P/\dot{T} \qquad (3)$$

(with t time and P power applied), shows the possibility of operation in dynamic modes. By keeping P or $\dot{T}$ constant, while increasing or decreasing the temperature of the sample (positive or negative values for P and $\dot{T}$), four practical modes of operation are obtained (*12–14*). These modes require different settings for the (adiabatic) thermal environment (thermal shields) of the sample. The most interesting modes are the ones with constant heating or cooling power P. As will be

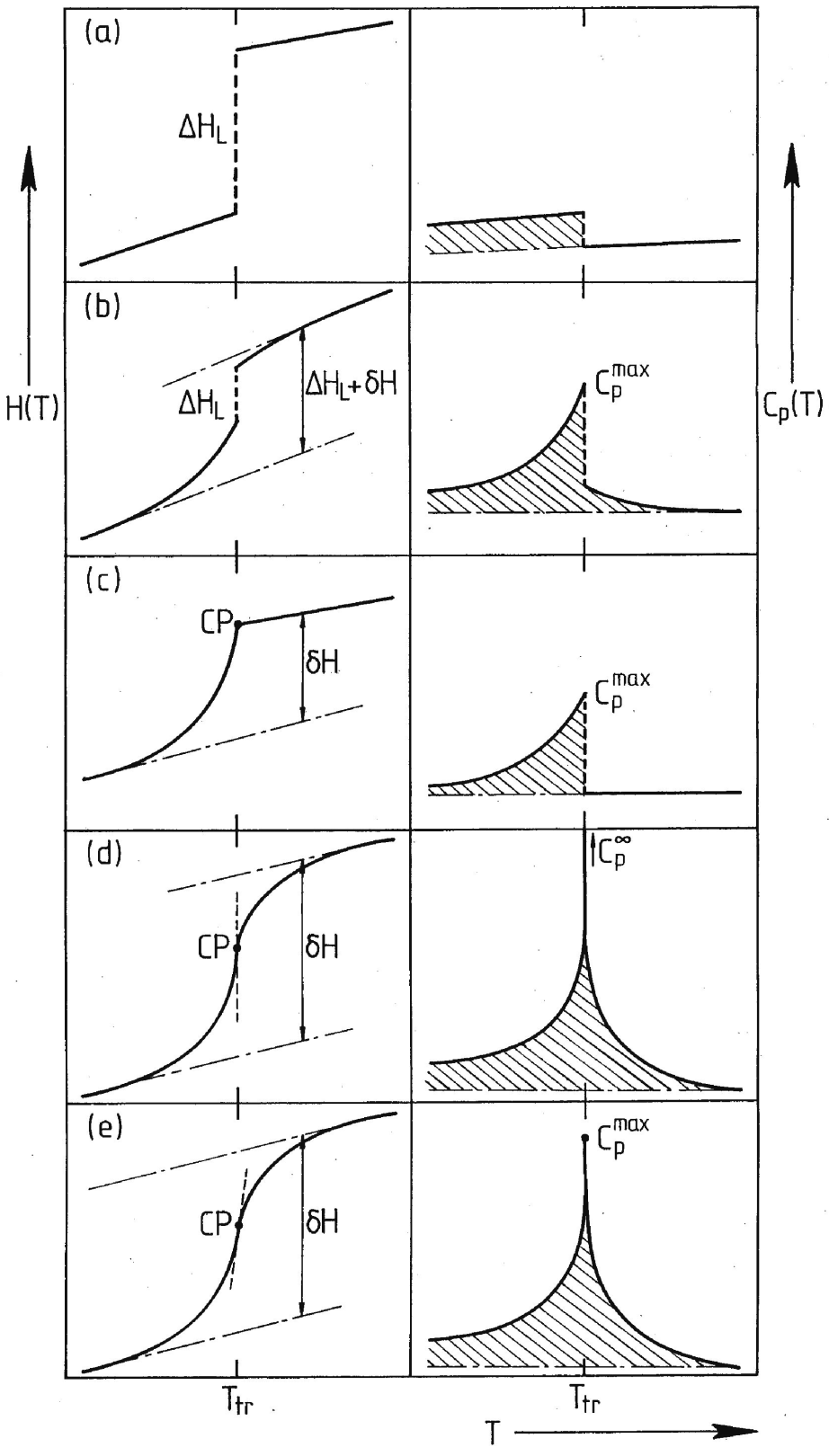

Figure 1. Schematic representation of the temperature dependence of the enthalpy H and the specific heat capacity C_p for different types of phase transitions at T_{tr}. (a) strongly first order; (b) weakly first order; (c) mean-field second order; (d) second order with diverging C_p; (e) second order with large but finite C_p. ΔH_L is the latent heat and δH the fluctuations induced pretransitional enthalpy change. CP indicates the critical point.

pointed out further, these modes have distinct advantages at first-order transitions. On the other hand, modes where $\dot{T}$ is kept constant have a basic problem (even at very low scanning rates, e.g. sub-mK min^{-1}) at a first-order phase transition, because a finite amount of heat (corresponding with the latent heat), necessary to maintain $\dot{T}$ constant cannot be delivered instantaneously. Rounding of effects will be the result. This problem occurs also, but more extremely, in differential scanning calorimetry (DSC) experiments, typically operating at constant rates of 1 to 10 K min^{-1} (*5*). Here we will only consider heating and cooling runs with the power P of Equation (3) kept constant (modes 1 and 3 in references (*12*) to (*14*), where a more detailed discussion is presented also on the constant rate modes). In the heating mode with constant (electrically applied) power P^e to the sample (cell), one has to arrange for a negligibly small leaking power P^l to the environment, measure P^e and carefully follow the evolution of the sample temperature $T(t)$ with time t. From $T(t)$ one can derive $\dot{T}$ by numerical differentiation and calculate C_p with Equation (3). Because the rate $\dot{T}$ is inversely proportional to C_p, at a second-order phase transition with an anomalous heat capacity increase the rate will decrease and thermodynamic equilibrium and servo control of adiabatic conditions is facilitated. First-order transitions also do not pose a problem because in principle the rate stays zero at the transition for a time interval given by:

$$\Delta t \equiv t_f - t_i = \Delta H_L / P^e, \tag{4}$$

with ΔH_L the latent heat of the transition. t_i and t_f are times during the scan at which the transition is reached and left, respectively. In fact, the direct experimental result $T(t)$ immediately gives the enthalpy as a function of temperature by:

$$H = H(T_s) + P^e(t - t_s), \tag{5}$$

with T_s the starting temperature of the scanning run at the time t_s. The implementation of a cooling run with constant (negative) power is less obvious and has to be realised by imposing a constant leaking power between the sample (cell) and its isothermal environment. This can be done by imposing a constant temperature difference. These conditions have to be verified and usually involve calibration (certainly when scanning over large temperature ranges) to arrive at absolute values for the heat capacity or enthalpy. This type of cooling run (with negative power and negative rate) is very similar to the constant power heating mode and also easily allows one to deal with first-order transitions. Although an ASC is normally optimised for scanning, it can easily be operated as a normal heat-pulse step calorimeter as well. This can be very practical for calibration purposes and verification of absolute heat capacity values.

3.2 Practical implementation

Very important in the operation of an ASC is the high-resolution measurement and control of the temperature. An essential feature is the elaborate effort one has to make to isolate the specimen (holder) from the laboratory by means of a precisely controlled thermal environment. To measure the heat capacity and enthalpy of a liquid (crystal) one needs at least a liquid cell and a surrounding (adiabatic) shield. However, for high-resolution and slow scanning rates two or more shields are required. Over many years we have constructed several ASCs. The differences resulted from adaptation to study specific types of samples, the extent of temperature range to operate or to allow for novel electronic controlling possibilities. In the past extensive analogue ac Wheatstone bridge-type controlling systems had to be used (*12,15–17*). However, the appearance during the last 10 to 20 years of fast PCs and measurement instrumentation with extensive interfacing capabilities as well as powerful software has significantly simplified the design of an ASC as well its operation, and as a result, it can run, if desired, for weeks without human interference.

Figure 2 gives a schematic diagram of a four-stage ASC that can operate between room temperature and about 470 K. The centrally located cylindrical sample cell is surrounded by three (copper) thermal shields. Each of the stages (1 to 4) has its own thermometer (Th_i) and its own electrical (e.g. constantan) heating wires. On stages 1 to 3 the heating wires are evenly distributed and wound in grooves, and thermally anchored with a good thermal conductive and electrically insulating epoxy. Stage 4 of this calorimeter is composed of a hot air oven and the outer thermal and vacuum shield of the actual calorimeter with three internal stages. The temperature of the oven is measured and controlled by means of the thermistor Th_4 and computer-regulated power delivery to the heater of the oven. The stages are in very poor thermal contact and the space between the stages is vacuum pumped. The sample cell is suspended by thin nylon threads inside stage 2. To minimise further thermal transfer between stages all electric connecting wires are, on passing from one stage to another, several thermal diffusion lengths long (for temperature variations at relevant time scales), and neatly coiled not to

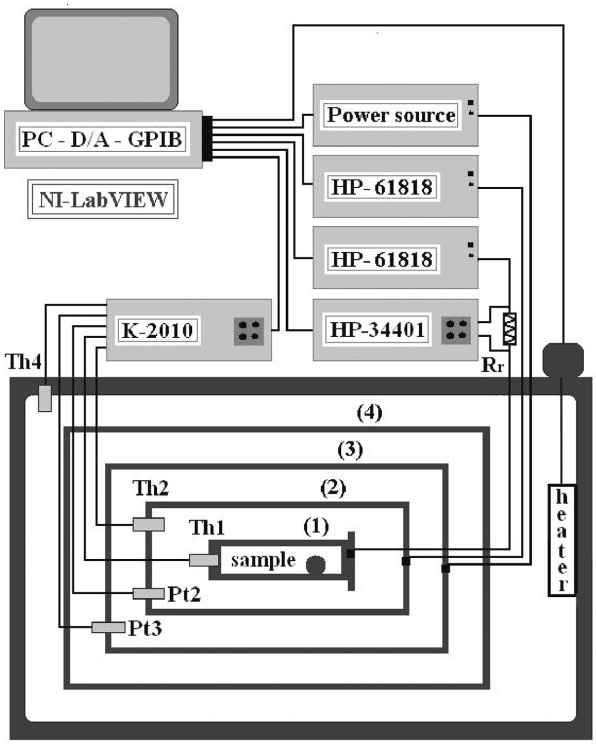

Figure 2. Schematic diagram of a four-stage ASC with typical modern measurement and PC-controlled instrumentation. (1): sample in sample holder with stirring ball, thermistor Th_1 and heater (not shown); (2): shield with thermistor Th_2, platinum reference thermometer Pt_2 and heater (not shown); (3): shield with platinum thermometer Pt_3 and heater (not shown); (4): external vacuum tight shield in hot air oven with thermistor Th_4 and heater. K-2010 (7.5 digits multiplexer) and HP-34401 (6.5 digits multiplexer) are multimeters. There are two HP-61818 power sources and one home-made one.

touch the wall of either stage. These wires are also thermally anchored at each stage.

One of the consequences of measuring liquids is the need for a (closed) sample holder. In order to achieve maximum sensitivity, the heat capacity of the holder should be as small as possible compared with that of the liquid sample. This can be easier realised with large samples and holders. However, for large samples internal relaxation times might become important even for slow scanning rates (*13*). In order to reduce possible temperature inhomogeneities, stirring the sample is very effective. In our calorimeters, stirring in the horizontally mounted cylindrical cells is achieved by means of a metal ball that can roll back and forth inside the cell by changing periodically the inclination of the plate supporting the calorimeter. For common liquids and some liquid crystals large samples (from a couple of grams to several tens of grams) could conveniently be used. For less common compounds we scaled down the size of the sample holders substantially. Presently our smallest cells contain 200 to 300 mg of sample and are made from tantalum or molybdenum for chemical inertness, good thermal conductivity and low heat capacity (*18*).

4. Data treatment and analysis

The basic data measured very frequently as a function of time (typically every 5 to 10 s) during a heating run in an ASC are the temperature of the sample and the holder as well as the (constant) power. These results are graphically displayed in the two central boxes of Figure 3 for a weakly first-order transition.

After a long temperature stabilisation time of stage 2 (shield around the sample cell) with zero power to the cell (stage 1), the cell attains the same temperature (within a few tenths of a mK). Then the power is switched on, at t_0, to a chosen value depending on the desired overall scanning rate. A typical run over a couple of degrees takes several days or weeks (for very slow scans). The temperature is measured with μK resolution and the extremely large number of $T(t)$ data allows averaging (if desired) and determination of local derivatives resulting in nearly as many $\dot{T}$ values as $T(t)$ data points by using several (consecutive) data points in a moving time derivative (adding one data point at one end and leaving out one at the other end). A simple division P by $\dot{T}$ at a given $T(t)$ results immediately in a $C_p(T)$ value at that temperature. One should realise that these $C_p(T)$ values are total heat capacities for the sample and the sample

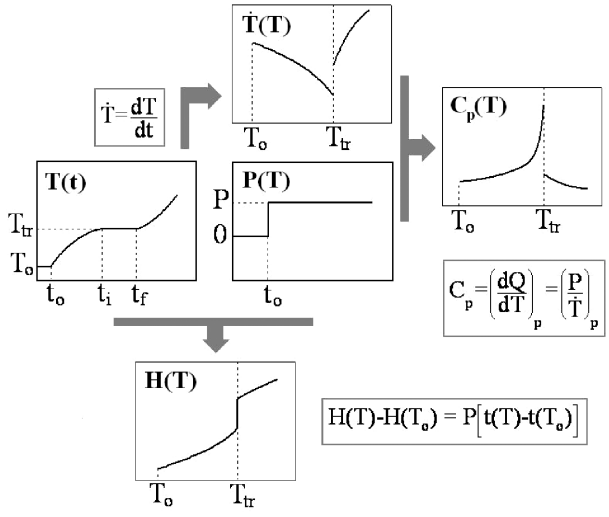

Figure 3. Illustration of the treatment of the directly obtained $T(t)$ and $P(t)$ data in a constant power heating run for a weakly first-order transition to arrive at results for the specific heat capacity $C_p(T)$ and the enthalpy $H(T)$. T_0 is the starting temperature at the time t_0. t_i and t_f are the beginning and the end of a first-order transition at T_{tr}.

holder together. Proper calibration of the (only weakly T-dependent) heat capacity of the empty cell and knowing the total amount of sample allows the calculation of the specific heat capacity of the sample. In the case of the weakly first-order transition, the transition is reached at time t_i. From that moment until t_f the temperature remains constant over the time interval given by Equation (4). According to Equation (5) the direct combination of $t(T)$ and $P(t)$ data immediately results in the enthalpy as a function of temperature, including the latent heat discontinuity for a first-order transition as displayed in Figure 3. The fact that in ASC the most direct result is $H(T)$ makes it a unique tool for determining the order of a phase transition. In Figure 3, at the first-order transition T versus t is depicted perfectly horizontal and H versus perfectly vertical. This is, however, an idealised situation for a perfectly pure one-component sample. For real systems, even with minute amounts of impurities, as well as for two or more component mixtures, one observes a two-phase region. For rather pure one-component systems this two-phase region is typically a couple of tens of mK, and depends on the impurity type and level and on the latent heat (*19*). ASC also allows accurate determination of the two-phase region.

As already indicated, second-order (continuous) phase transitions are characterised by large fluctuations, which for a properly defined order-parameter diverge in size to infinity. The divergence of the size of the fluctuations can be described by a power law with a characteristic critical exponent depending on the universality class of the phase transition (*20*). Also the limiting behaviour of the specific heat capacity at a second-order transition can be described by means of a power law of the form:

$$C_p = A|\tau|^{-\alpha}+B, \tag{6}$$

with $\tau = (T - T_c)/T_c$, A the critical amplitude, α the critical exponent, T_c the critical temperature and B the background. In a constant power heating or cooling run one readily arrives at the heat capacity C_p in Equation (3) from the (known) power and the temperature-depending rate by numerical differentiation of $T(t)$, the carefully measured temperature evolution of the sample with time. However, the fact that via Equation (5) $T(t)$ can immediately be transformed in an enthalpy versus temperature curve opens new possibilities for data analysis. This can best be illustrated using Figure 4 with a generic enthalpy curve for a continuous phase transition.

At the temperature T with a corresponding enthalpy $H(T)$, two quantities with dimensions (J kg^{-1} K^{-1}) of a specific heat capacity, C_p and C, are introduced. C_p corresponds to the slope, dH/dT, of the enthalpy curve at T, and C is defined as:

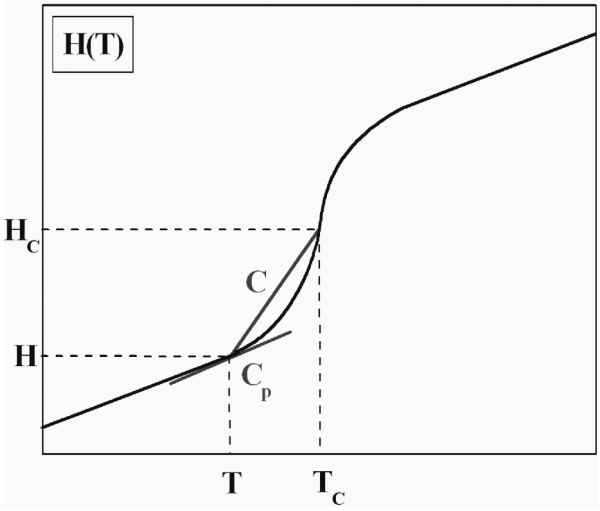

Figure 4. Generic enthalpy curve near a second-order phase transition at $H_c(T_c)$. The slope of $H(T)$ at a temperature T corresponds to C_p and the slope of the chord between $H(T)$ and H_c corresponds to C.

$$C = \frac{H - H_c}{T - T_c}, \tag{7}$$

and thus corresponds to the slope of the chord connecting $H(T)$ at T with H_c at T_c. It can easily be shown that C also has a power law behaviour of the form (*16,17*):

$$C = \frac{A}{1-\alpha}|\tau|^{-\alpha}+B. \tag{8}$$

Thus, both C_p and C have the same critical exponent and background term, but a different critical amplitude. Either Equation (6) or (8) can be used for (non-linear) curve fitting of the experimental data to arrive at important values for the critical exponent α and amplitude A. However, by considering the difference $(C - C_p)$, above or below T_c, the (unimportant) background term drops out, resulting in:

$$C - C_p = \frac{\alpha A}{1-\alpha}|\tau|^{-\alpha}. \tag{9}$$

Taking the logarithm on both sides of Equation (9) gives:

$$\log(C - C_p) = \log\left(\frac{\alpha A}{1-\alpha}\right) - \alpha\log|\tau|. \tag{10}$$

Thus, one obtains a straight line with a (negative) slope immediately giving the critical exponent α.

Applications of this procedure for several phase transitions will be given further.

5. Isotropic to nematic and to smectic A transitions

In this section, ASC results concerning the transition to the nematic phase from the isotropic or directly to the smectic A phase for some compounds will be considered. The only difference between the isotropic phase and the nematic phase is the orientational order of the long molecular axes of the (calamitic) liquid crystalline compounds. A proper description of this orientational order requires the introduction of a tensor of the second rank (*1,2*). This tensor can be diagonalised, and for anisotropic liquids with uniaxial symmetry the nematic phase can be described by only one scalar order parameter. For biaxial symmetry, a second independent order parameter is required. In the vicinity of the nematic-to-isotropic (NI) transition the thermodynamic behaviour is usually described with the Landau-de Gennes mean-field theory. For a uniaxial nematic liquid crystal one writes the free energy F as an expansion of the modulus of the order parameter S:

$$F = F_0 + \frac{1}{2}A_0S^2 - \frac{1}{3}B_0S^3 + \frac{1}{4}C_0S^4 + \frac{1}{6}D_0S^6 + \ldots . \quad (11)$$

In the isotropic phase, $S = 0$ and $F = F_0$, and in the nematic phase $S \neq 0$. In Equation (11) one has $B_0 > 0$ and $A_0 = a(T - T^*)/T_{NI}$, with $a > 0$ and T^* the stability limit of the isotropic phase. The presence of the cubic term leads to a first-order transition at T_{NI} with a finite discontinuity, $S_{NI} = 2B_0/3C_0$ in the order parameter. The excess heat capacity in the nematic phase is given by (*21*):

$$C_p = -aS\left(\frac{\partial S}{\partial T}\right)_p = \frac{a^2}{C_0T_{NI}}\left[1 + \frac{B_0}{2(aC_0)^{1/2}}\left(\frac{T^{**} - T}{T_{NI}}\right)^{-1/2}\right], \quad (12)$$

with T^{**} the stability limit of the nematic phase. At the NI transition temperature T_{NI} there is a jump in C_p equal to $\Delta C_p = 2a^2/C_0T_{NI}$. For the enthalpy discontinuity (latent heat) at T_{NI} one obtains:

$$\Delta H_L = H_I - H_N = 2aB_0^2/9C_0^2. \quad (13)$$

Due to the presence of the (small) cubic term in Equation (11), the NI transition is predicted to be (weakly) first order. This is in agreement with experimental observations. In Figure 5, part of the enthalpy curve near T_{NI} is shown for pentylcyanobiphenyl

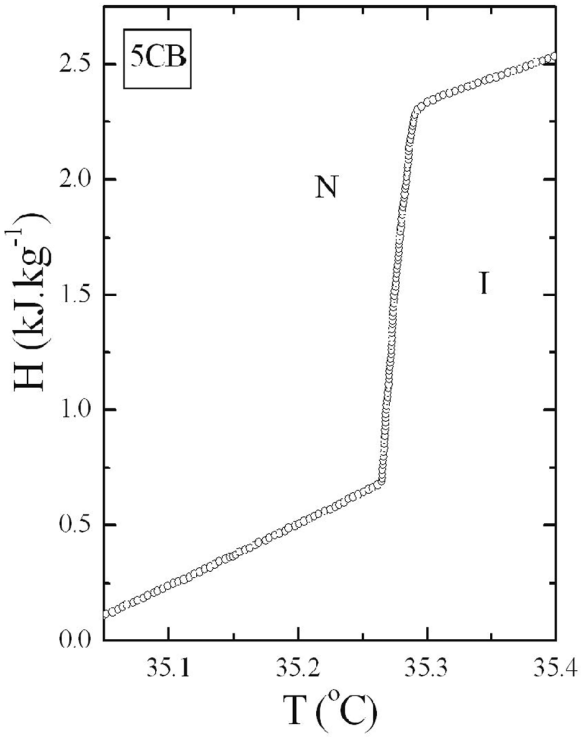

Figure 5. Temperature dependence of the enthalpy near the nematic-to-isotropic transition for pentylcyanobiphenyl (5CB).

(5CB), a compound of the alkylcyanobiphenyl (*n*CB) homologous series (*22,23*). The transition is clearly first order with a latent heat of 1.56 ± 0.01 J g^{-1}.

In the past ASC measurements on all the *n*CB compounds from 5CB to 11CB have been done (*17,22–24*). Recently we also measured 12CB, 13CB and 14CB (*25,26*). It should, however, be noted that the higher homologous 10CB to 14CB exhibit a direct transition from the isotropic phase to the smectic A (SmA) phase. At this transition additionally one-dimensional positional order is superimposed on the overall (nematic-like) orientational order and these transitions are also first order. Moreover, latent heats turn out to be substantially larger than for NI transitions in the same homologous series. This can be observed in Figure 6 where for the *n*CB compounds from 5CB to 14CB parts of the enthalpy curves near the NI or N–SmA are presented.

Figure 7 gives an overview of the transition temperatures and latent heats for the isotropic-to-nematic (IN) and isotropic-to-smectic A (I–SmA) transitions for the *n*CB homologous series. For $n \leq 9$, one has NI transitions and for $n \geq 10$ one has I–SmA transitions. The NI transitions have rather small latent heats that show the characteristic odd–even effect also visible

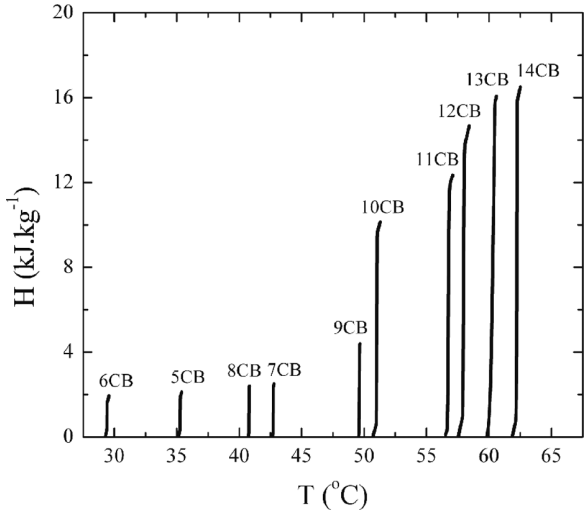

Figure 6. Parts of the enthalpy as a function of temperature near the isotropic to nematic transitions for 5CB to 9CB and near the isotropic to smectic A transitions for 10CB to 14CB. The data for 13CB have been shifted down by 2°C in order to avoid overlap with the 14CB data.

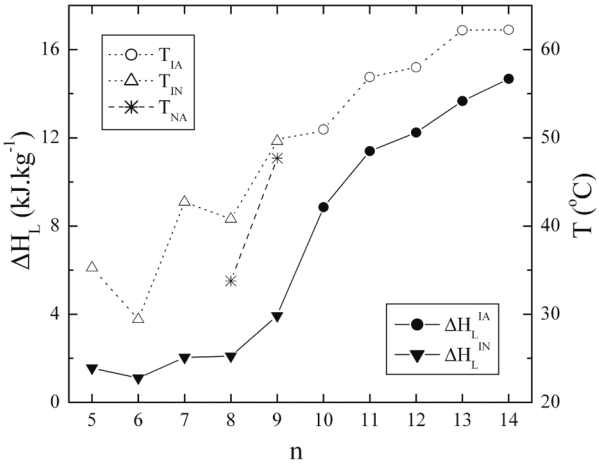

Figure 7. Latent heats (filled symbols and solid line) and transition temperatures (open symbols and dashed line) as a function of the number of carbon atoms in the alkyl chain in the alkylcyanobiphenyl (*n*CB) homologous series. Circles are isotropic-to-nematic transitions and triangles are isotropic-to-smectic A transitions. The stars indicate the nematic to smectic A transitions for 8CB and 9CB.

in the transition temperatures. The latent heats for the I–SmA are substantially larger and the odd–even effect is less pronounced for the latent heats than for the transition temperatures. In Table 1 values of the transition temperature, latent heats and the widths of the two-phase region are given for all the *n*CB compounds studied by ASC.

The latent heat values in Table 1, in particular for the IN transition, are quite small and about two orders

Table 1. Overview of phase transition parameters for the cyanobiphenyl (*n*CB) homologues series.

*n*CB	T_{IN},T_{IA} (°C)	ΔT_{coex} (mK)	L_{IN},L_{IA} (kJ kg^{-1})
5	35.29[a]	25[b]	1.56[b]
6	29.42	13	1.10
7	42.73	12	2.03
8	40.80	14	2.14
9	49.64	50	3.9
10	51.04	80	8.9
11	56.93	300	11.4
12	58.19	180	12.2
13	62.20	780	13.7
14	62.25	180	14.7

[a]The transition temperatures are for the first appearance of the mesophase in cooling runs.
[b]The uncertainty is estimated to be 2%.

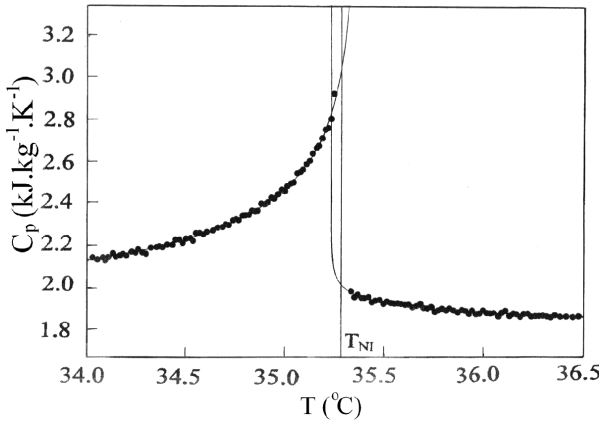

Figure 8. Pretransitional heat capacity in the isotropic and the nematic phase near the isotropic-to-nematic phase transition of pentylcyanobiphenyl (5CB).

of magnitude smaller than the latent heats at the melting transitions in the *n*CB compounds (*17,24–26*). Thus, these transitions are close to second order and one might expect fluctuation effects resulting in many physical properties exhibiting critical point-like behaviour described by power laws with appropriate critical exponents. This is, indeed, the case for many properties including the specific heat capacity. Figure 8 gives the temperature dependence of C_p near the NI transition for pentylcyanobiphenyl (5CB). Power law fits with equations of the form given by Equation (6) can be carried out to fit these and similar data to arrive at critical amplitudes and exponent values. However, fits with Equation (6) must be made separately above and below T_{NI} with different effective critical temperatures (T^* and T^{**}) that are different from the first-order transition temperature at T_{NI}. Fits to C_p data for several compounds (*17,22,23,27,28*) with expressions of the type of Equation (6) are strongly dependent on the fitting range. For the data in the nematic phase

effective critical exponent α values are in the range 0.3 to 0.5. In the isotropic phase the uncertainty on the effective α values is even larger (between 0.1 and 0.5) because of the substantially smaller pretransitional increase. Efforts to fit the smaller pretransional contributions at the stronger first-order I–SmA transition are even less satisfactory. Several other exponents, in particular the order parameter exponent β, seem to be close to the tricritical value, 0.25 for β (*29*). Keyes (*30*) and Anisimov et al. (*31,32*) formulated arguments that indeed tricritical values should be expected. Keyes invoked the presence of two competing order parameters (uniaxial and biaxial ones) that are expected to exhibit diverging fluctuations near T_{NI} even for an on average zero biaxial order parameter. Anisimov et al. argued that the behaviour looks like that near a tricritical point because of the smallness of the coefficient C in the Landau expression of Equation (11). A specific crossover expression between tricritical (α = 0.5) and Ising-critical (α = 0.11) was also proposed for the specific heat capacity by Anisimov et al (*32*). Good fits to the data could be obtained with that expression (containing several adjustable parameters) (*27,22,23*). This is illustrated in Figure 8 where the solid lines through the experimental data are based on such a fit (*22,23*). However, conflicting results are obtained for the same parameters in fitting equations when deduced from measurements of different physical properties. For example, the values for ($T^* - T_{NI}$) and ($T^{**} - T_{NI}$) obtained from C_p data are consistently about one order of magnitude smaller than values derived from several other physical quantities. Thus, more involved (theoretical) approaches seem to be needed to fully understand the isotropic-to-nematic transition or the isotropic-to-smectic A transition.

6. Smectic A to nematic transitions

The transition from the nematic (N) to the smectic A (SmA) phase is probably the most extensively studied phase transition in liquid crystals (*33*). However, in spite of vigorous experimental and theoretical efforts, many aspects of it are not yet understood, making this transition still an intriguing and challenging problem in the statistical mechanics of soft condensed matter.

In addition to orientational order, the smectic A phase exhibits one-dimensional positional order (one-dimensional density wave) as well. The first theoretical efforts to describe the simultaneous existence of orientational and positional order resulted in the (mean field) molecular models formulated by Kobayashi (*34*) and McMillan (*35*). A couple of years later de Gennes (*36*) showed that the basic aspects of these models could be represented by a Landau free energy expansion with an additional coupling between the smectic density-wave amplitude ψ and the scalar nematic order parameter S. The one-dimensional smectic density-wave (with a wave vector parallel to the director along the z-axis) is characterised by a two-component complex order parameter $\psi.exp(i\varphi z)$ with magnitude ψ and phase φ. It was shown by de Gennes that the behaviour of this two-component order parameter near the N–SmA transition was very similar to that at the normal-superconductor transition (*36,37*). Thus one expects the N–SmA transition (in the absence of coupling between the nematic and smectic order parameters) to belong to the 3D-XY universality class (*1,20*).

In the cases we consider here the coupling between nematic and the smectic A order parameters is important. For this reason we will give a summary of the de Gennes theory involving the de Gennes S-ψ coupling. The relevant free energy density expansion is:

$$F = F_N(S) + \frac{1}{2}\alpha(T)\psi^2 + \frac{1}{4}\beta\psi^4 - C\psi^2\delta S + \frac{1}{2\chi}\delta S + \dots . \quad (14)$$

F_N is the nematic free energy density given by Equation (11). For $T < T_{N\text{–}SmA}$, one has $\delta S = S - S_0$, with $S_0(T)$ the nematic order parameter in the absence of smectic order. The temperature dependence of α is given by $\alpha(T) = \alpha_0(T - T_0)$. χ is a temperature-dependent nematic susceptibility that is large near T_{NI} but decreases with decreasing temperature. α_0, β, and C are positive constants. On minimising F with respect to δS, one gets $\delta S = C\chi\psi^2$; and then eliminating δS from F yields:

$$F = F_N(S) + \frac{1}{2}\alpha(T)\psi^2 + \frac{1}{4}\beta'\psi^4 + \dots , \quad (15)$$

with:

$$\beta' = \beta - 2C^2\chi. \quad (16)$$

Depending on the values of C and χ and the resulting sign of β' three different cases can be obtained. For $\beta' > 0$ one has a continuous transition with $T_0 = T_{N\text{–}SmA}$, $\beta' < 0$ corresponds to first-order transitions, and at $\beta' = 0$ one has the crossover from (second-order) continuous transitions to first-order transitions at the tricritical point.

For pure compounds with $T_{N\text{–}SmA}$ close T_{NI} (narrow nematic range) one expects a large χ value and a negative β' value resulting in a first-order transition at $T_{N\text{–}SmA}$. On the contrary, for large nematic ranges χ will be small at $T_{N\text{–}SmA}$ and β' positive. The N–SmA transition will be second order. This difference in the

order of the N–SmA transition can be illustrated by looking at 8OCB and 9OCB, two compounds of the octyloxycyanobiphenyl homologous series. 8OCB has a nematic range of 13.1 K and the N–SmA transition is second order within experimental resolution (*38*).

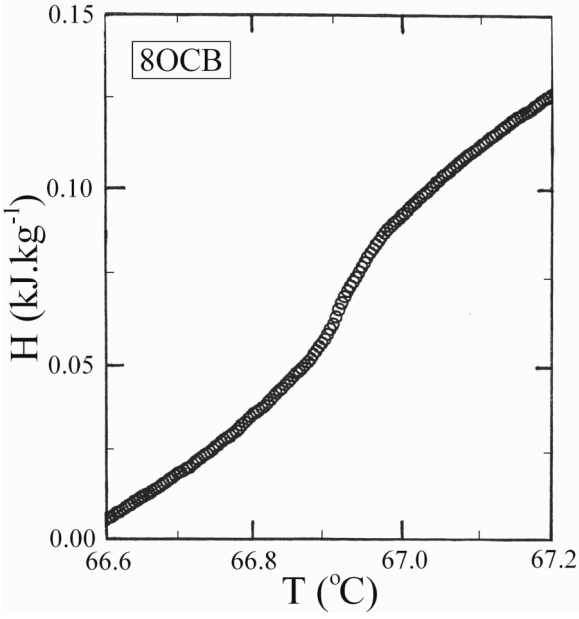

Figure 9. Temperature dependence of the enthalpy near the N–SmA transition of 8OCB. Within experimental resolution the transition is second order (with an upper limit for a possible latent heat of 1.8 J kg^{-1}).

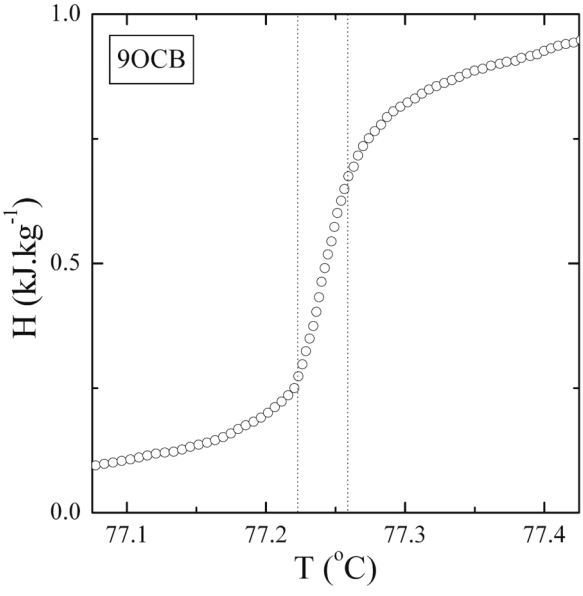

Figure 10. Temperature dependence of the enthalpy near the N–SmA transition of 9OCB. The transition is clearly (weakly) first order with a latent heat of 0.46 ± 0.05 kJ kg^{-1} and a two-phase region of 35 ± 2 mK.

9OCB, with a nematic range of 2.17±0.05K, on the other hand, is clearly first order with a latent heat of about 0.46 ± 0.05 kJ kg^{-1} (*39*). In Figures 9 and 10, the enthalpy as a function of temperature near T_{N-SmA} is displayed for the pure compounds 8OCB and 9OCB, respectively.

Finding the condition $\beta' = 0$ for the N–SmA transition and thus exactly being at a tricritical point for a pure compound would be a lucky accident, although for 9CB (nonylcyanobiphenyl) it is very close (*40,41*). However, by mixing two liquid crystal compounds (usually of the same homologous series), one with a narrow nematic range (and a first-order N–SmA transition) and one with a sufficiently wide nematic range (and a second-order N–SmA transition), it is possible to arrive at a given mole fraction x to obtain the proper width of the nematic range for $\beta' = 0$ and a tricritical point. ASC has been used extensively to study in great detail the thermal behaviour along the second-order and first-order parts along the $T_{N-SmA}(x)$ line as well as at the tricritical x (*40,41*). The fact that in ASC the direct result is the enthalpy as a function of temperature, and can discriminate between first-order and second-order transitions, allows accurate location of the tricritical point.

With ASC one simultaneously obtains high-resolution data on the fluctuations-induced specific heat capacity anomalies near the N–SmA transitions. If one characterises these anomalies in terms of the specific heat capacity critical exponent α in Equation (6), there are many liquid crystals that lie, because of de Gennes order parameter coupling, in the crossover region between tricritical with $\alpha = 0.5$ and second-order 3D-XY with $\alpha = \alpha_{XY} = -0.013$ (*13,33*). In

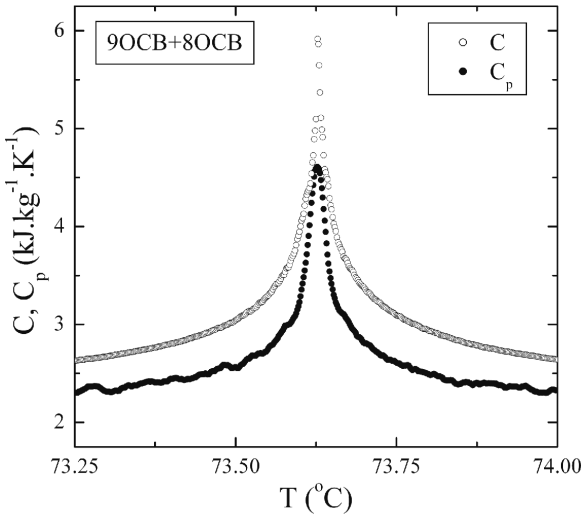

Figure 11. Plots for the specific heat capacity C_p and the quantity C of the Equations (7) and (8) near T_{N-SmA} for a mixture of 8OCB + 9OCB with mole fraction $x_{8OCB} = 0.55$.

order to arrive at accurate values for the (effective) α critical exponent, the difference in Equation (9) between the slope C_p of $H(T)$ and of the slope C of the chord (in Figure 4) at a temperature T is extremely useful because the background is eliminated and linear curve fitting can be done with Equation (10). Figure 11 displays the quantities C_p and C near the N–SmA transition in a mixture of 8OCB+9OCB with mole fraction $x_{8OCB} = 0.55$.

Within experimental resolution the transition is second order (*39*). In Figure 12 $\log(C - C_p)$ is plotted versus $\log|\tau|$ resulting in an effective α value of 0.34 ± 0.03, as given by the negative slope (see Equation (10)). This value is substantially larger than $\alpha = 0.18 \pm 0.02$ for the second-order N–SmA transition of 8OCB (*38,42*). Thus, modifying the de Gennes coupling between the order parameters S and ψ by changing the width of the nematic range in mixtures of liquid crystals can result in a change in the order of the N–SmA transition as well as in large changes of the effective heat capacity critical exponent α along the second-order part of the $T_{N-SmA}(x)$ line. Narrow nematic ranges result in first-order transitions and wide nematic ranges in second-order ones with decreasing effective critical exponents α with increasing width of the nematic range.

The situation is, however, quite different when chirality plays a role. It was theoretically suggested (*43,44*) that chirality always drives the chiral nematic-to-smectic A (N*-SmA) transition first order. A few years ago this theoretical prediction was verified in an ASC investigation (*38*). This transition was studied in mixtures of the non-chiral liquid crystal 8OCB and the chiral CB15 (4-(2-methylbutyl)-4'-cyanobiphenyl), a binary system with a large (chiral) nematic range that widens upon increasing the chiral (CB15) fraction. Since 8OCB has

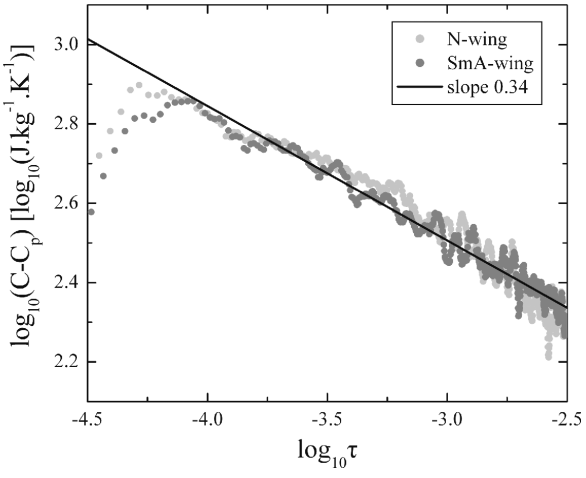

Figure 12. Plots of $\log_{10}(C - C_p)$ versus $\log_{10}|\tau|$ below and above T_{N-SmA} for the mixture of 8OCB + 9OCB (of Figure 11) with mole fraction $x_{8OCB} = 0.55$.

no measurable latent heat (see above), and taking into account the widening of the chiral nematic range, the possibility of a second-order to first-order crossover due to an increased S-ψ coupling can be excluded. For all examined mixtures a latent heat could be determined at the N*-SmA transition. The latent heat increased with increasing mole fraction of the chiral compound. Although the qualitative theoretical prediction of the first-order character of this transition was confirmed, the predictions of the evolution of the enthalpy or entropy discontinuities were not consistent with the experimental results (*38*).

Non-mesogenic additions can also have a profound impact on the N–SmA transition of a liquid crystal. Recently we studied, by means of ASC, the effects of the non-mesogenic solutes cyclohexane (CH), biphenyl (BP) and water (W) on the N–SmA (as well as on the NI) transition of 8CB (octylcyanobephenyl) (*45,46*). 8CB exhibits a NI transition at 41.7°C and a N–SmA transition at 33.7°C. Within experimental resolution the N–SmA transition is second order with an effective critical exponent $\alpha = 0.31 \pm 0.03$ (*17*). For BP and CH a linear decrease of the NI and N–SmA transition temperatures was observed with increasing solute mole fraction. For 8CB+BT the width of the nematic range increased with increasing mole fraction of BP. For 8CB+CH, on the contrary, the width of the nematic range decreased with increasing mole fraction of CH. For water the transition temperatures stayed nearly constant (after a slight decrease for mole fractions of water up to 0.1). For 8CB+W the nematic range slightly increased up to $x_W = 0.1$ and stayed constant above that value. For water it was found that for mole fractions of water above 0.1 phase separation between an 8CB-rich phase and a water-rich phase occurred. For BP mole fractions of biphenyl and water studied, the N–SmA transition remains second order. For 8CB+CH crossover from second order to first order is observed at a tricritical point of the mole fraction x_{CH} of CH around 0.046. Above this mole fraction the latent heat of the first-order N–SmA transition rapidly increased with increasing x_{CH}.

In Figure 13, the enthalpy is given as a function of temperature for a mixture of 8CB+CH with a mole fraction of $x_{CH} = 0.079$. The latent heat discontinuity is clearly visible at this first order transition. As illustrated in Figure 14 the effective critical exponent α values at the N–SmA transitions of 8CB+BP decrease with increasing x_{BP}. Along the second-order part of the $T_{N-SmA}(x)$ line for 8CB+CH the effective critical exponents α values increase with increasing x_{CH} from the value of 0.31 for pure 8CB to the tricritical value of 0.5 for x_{CH} around 0.046. For 8CB+W the α value is nearly constant after a slight increase to a value of 0.36. The changes in the transition temperatures and

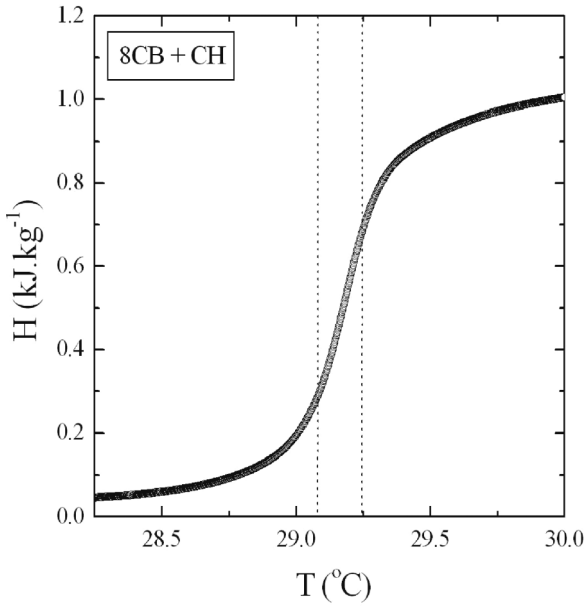

Figure 13. Temperature dependence of the enthalpy near the first-order N–SmA transition (with a two-phase region of 165 mK) in a mixture of 8CB and cyclohexane with a cyclohexane mole fraction of 0.079.

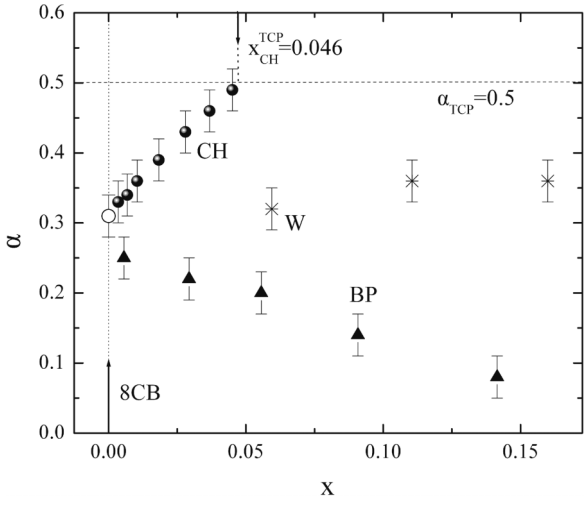

Figure 14. Mole fraction x dependence of the effective critical exponent α for 8CB and cyclohexane (CH), biphenyl (BP) and water (W), respectively.

differences between these three systems, and in particular the crossover from second order to first order for 8CB+CH, could be explained in terms of a mean-field free energy density expression including coupling terms of the mole fraction of the solutes with the nematic and smectic A order parameters (*46*).

The addition of nanoparticles can have a significant impact on the phase transitions in liquid crystals, in particular on the nematic-to-smectic A transition. Very recently we studied by ASC measurements the effects of magnetic nanoparticles with different surface coatings on the phase transitions of 8CB (*47*). Spherical nanoparticles with a core diameter of 2 nm and different surface coatings were used for this study. Two mixtures of 8CB and the nanoparticles with an identical concentration (30.6% wt) were prepared. In the first case (T1), the nanoparticles were coated with aminopropyltriethoxysilane (APTS) and in the second case (T2) with mercapto hexadecanoic acid (MHDA). For both mixtures, apart from a decrease in the transition temperatures, a shrinkage of the nematic range was observed, which is strongly dependent on the surface coating. ($T_{NI} - T_{N\text{–}SmA}$) equals 6.63 K for T1 and 5.27 K for T_2, compared with 7.03 K for pure 8CB. The NI transition remains weakly first order while the N–SmA transition is second order with larger effective critical exponents (α = 0.35 for T1 and α = 0.39 for T2) than for pure 8CB (α = 0.31). This increase scales with the decrease of the width of the nematic range and apparently enhanced coupling between the nematic and smectic A order parameters, similar to what was observed in the case of a non-mesogenic solute dispersed in the same liquid crystal compound (*45,46*).

The influence of adding magnetic nanoparticles is quite different from the effects induced by (hydrophilic) silica aerosil nanoparticles (typically 7 nm in diameter) that form a thixotropic gel when dispersed in a liquid crystal. In recent years, there have been several detailed calorimetric studies on these kinds of systems (*48–53*). The gel network induces quenched random disorder that destroys the quasi-long-range order in the SmA phase, but determining the effective critical exponents α at the N–SmA transitions is still possible. The presence of the aerosil gels does not significantly change the transition temperatures or the width of the nematic range. There is, however, a profound effect on the de Gennes coupling between the nematic and smectic A order parameters (S-ψ). There is a very different behaviour between random aerosil gels and (strong magnetic field) aligned aerosil gels. For random gels (*48–51*), there is a slow shift from the (effective) α value of the pure liquid crystal as aerosil density ρ_S increases, until α reaches the 3D-XY value at ρ_S = ~0.1. In the case of 8CB in aligned aerosil gels, the de Gennes coupling is completely absent and α_{XY} values are obtained for all investigated aerosil densities (*52,53*). Thus, the effects on the de Gennes coupling (S-ψ) of aerosil nanoparticles are completely different from the effects observed for systems with magnetic nanoparticles, with non-mesogenic solutes as well as in (binary) mixtures of liquid crystals. All these different observations infer a need for theoretical efforts for understanding not only the induced disorder but also

for a better understanding of nematic-to-smectic A transition.

7. Chirality, blue phases, TGB phases and transitions

When calamitic liquid crystal molecules lack left–right symmetry and the two types of handedness are not equally present in the sample, additional diversity in polymorphism occurs. In the chiral nematic phase (N*) or cholesteric phase the molecular orientation is nematic-like, but on a large scale (compared with the molecular dimensions) the director orientation acquires a spontaneous twist about an axis normal to the preferred local molecular direction. The helical pitch in the N* is substantially larger than molecular dimensions and varies with the type of molecule. For long pitch, one has a direct (weakly) first-order transition to the isotropic phase similar to the normal NI transition. For chiral nematics with short pitch (typically less than 500 nm), one can observe as many as three so-called blue phases between the isotropic and the normal cholesteric phase. In order of increasing temperature they are named BP_I to BP_{III}. The first two blue phases have three-dimensional cubic structures, whereas BP_{III}, which is also called the fog phase, appears to be amorphous (*54–56*). Phase transitions involving blue phases are expected to be first order, except for the isotropic to BP_{III} transition, which can become second order in an isolated critical point at the termination of a first-order line (*57*).

Figure 15 shows C_p results of cholesteryl nonanoate (CN) as obtained with ASC (*58*). From this figure it is clear that there is a substantial heat capacity effect

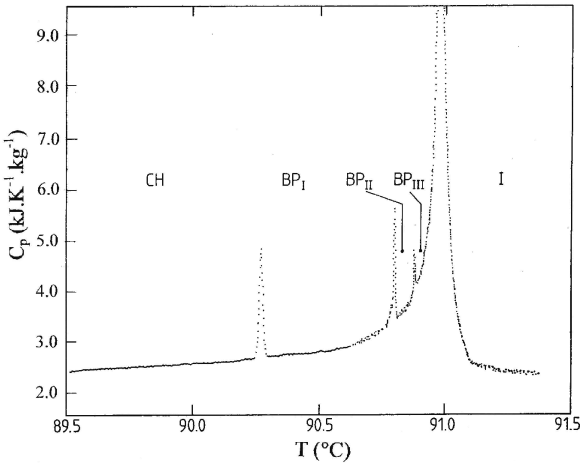

Figure 15. General overview of the specific heat capacity for a temperature range covering all phase transitions involving the blue phases of cholesteryl nonanoate.

associated with the isotropic-to-BP_{III} transition. This indicates that a large amount of energy is going into changing the local nematic order. The other transitions appear as small features on the I-BP_{III} transition peak. From a detailed inspection of the enthalpy behaviour (the direct ASC result) it was found that these small peaks correspond with very small latent heats: 34 ± 2 J kg^{-1} for N* – BP_I, 11 ± 1 J kg^{-1} for BP_I – BP_{II} and 3.6 ± 0.9 J kg^{-1} for BP_{II} – BP_{III}. With a value of 322 ± 47 J kg^{-1} the latent heat at the I-BP_{III} transition is much larger (*58*). The first calorimetric evidence for a continuous I-BP_{III} transition was obtained by Kutnjak et al. (*59*) in an ac and non-adiabatic scanning calorimetry investigation of the highly chiral compound S,S-(+)-4''-(methylbutyl) phenyl-4'-(methylbutyl)-4-biphenylcarboxylate (S,S-MBBPC). Subsequent studies of mixtures of S,S-MBBPC and its racemate identified a first-order line ending in a critical point (*60*). It could also be shown (*61*) that this critical point belongs to the Ising universality class as theoretically predicted (*62*).

The chirality of constituent molecules can also have significant effects on smectic phases. In tilted phases the chirality of the molecules will impose a twist axis normal to the smectic layers. A different type of chirality-induced smectic phase is the so-called TGB (twist grain boundary) smectic phases (*63–65*). These phases are composed of smectic blocks (or grains) separated by defects. The director (perpendicular to the layers) is rotated by a constant angle on going from one block to the next. Thus the helical axis is parallel to the smectic layers. Depending on the orientation of the molecules there are different TGB phases, e.g. TGB_A, or TGB_C.

Blue phases are normally found between the isotropic liquid and a chiral nematic phase of sufficiently short pitch in the sequence N*-BPs-I, except in a few cases where a direct BP_I–SmA transition has been observed (*66,67*). Some years ago we investigated by ASC mixtures of (R) and (S) enantiomers of the chiral compound ((R) or (S)-1-methylheptyl 3'-fluoro-4-octadecyloxybenzoyloxy)tolane-4-carboxilate), synthesised by Li et al. (*68*), with a phase sequence SmC*-TGB_c-TGB_A-BPs-I (*69*). It was found that all phase transitions, with the exception of the BP_{III} to isotropic transition, are clearly first order. The BP_{III} to isotropic transition peak showed a clear evolution (see Figure 16) from a broad supercritical $C_p(T)$ increase at low (S) fractions to a sharp first-order transition at the highest investigated (S) fractions.

From this evolution one expects the first-order line to end at a critical point in the vicinity of 10.5 % (S). These observations are in line with BP_{III} to isotropic transitions with an underlying N* phase instead of a TGB_A phase, as the case here. However, the general

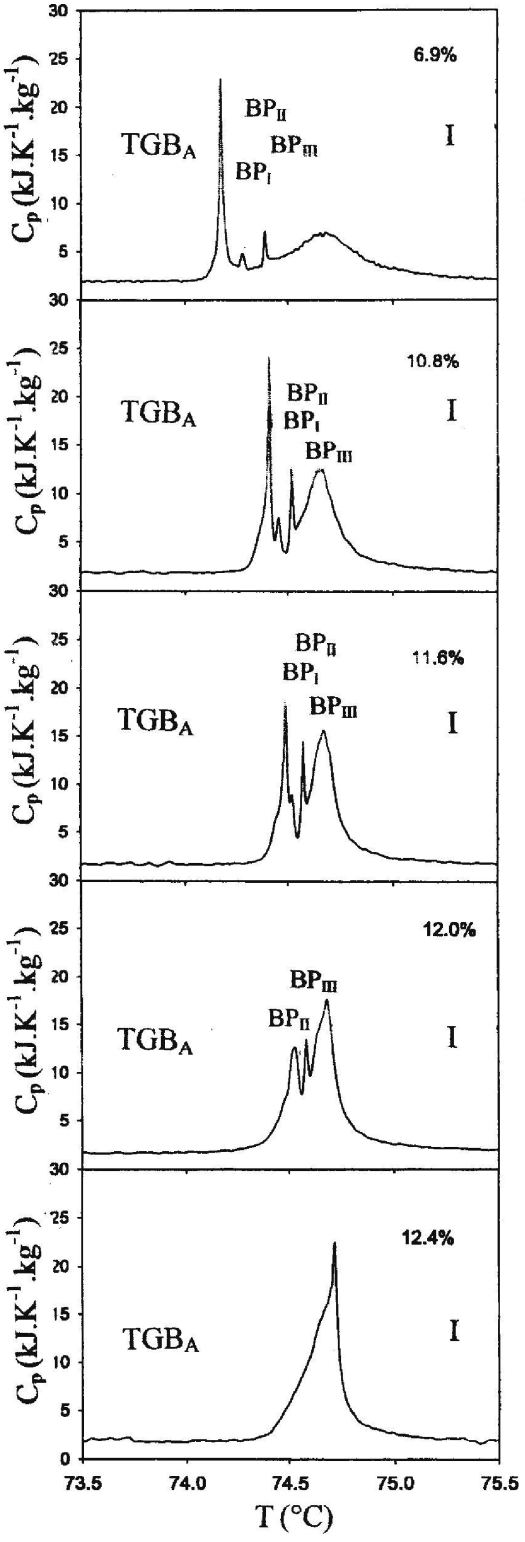

Figure 16. Evolution of the specific heat capacity in mixtures of ((R) and (S)-1-methylheptyl 3'-fluoro-4-octadecyloxybenzoyloxy) tolane-4-carboxilate) in the TGB_A-BPs-I region with increasing (S) enantiomer concentration. The supercritical BP_{III}-I C_p anomaly at low (S) concentrations evolves to a first-order transition at higher (S) concentrations through a critical point around 10.5%.

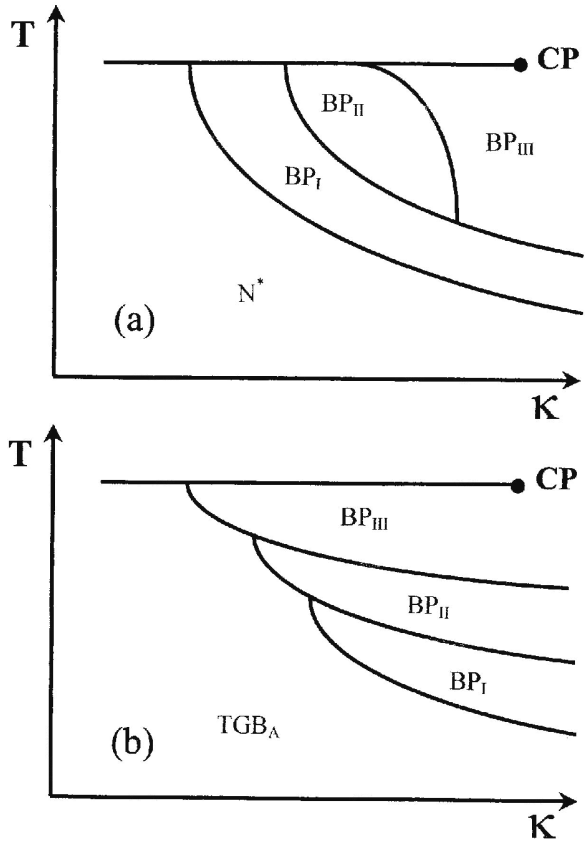

Figure 17. General form of the temperature (T) versus chirality (κ) phase diagram involving blue phases (a) as normally found in literature with a N* phase present and (b) as obtained from our ASC experiments with the N* phase replaced by a TGB_A phase.

shape of the phase diagram derived from our data is quite different from what is known in the literature (*62,70*). A qualitative comparison between the two types of phase diagrams is made in Figure 17. This is the first time that this novel phase diagram has been observed to our knowledge and a theoretical investigation would be useful.

8. Summary and concluding remarks

After presenting some general aspects of the specific heat capacity and enthalpy behaviour near first-order and second-order phase transitions, we discussed the different modes of operation of an ASC, its practical implementation and the data treatment and analysis. Results for the following types of liquid crystalline phase transitions were discussed in some detail: the isotropic to nematic and smectic A transitions; the nematic to smectic A transitions in pure compounds, in mixtures with other liquid crystal and with non-mesogenic solutes and in dispersions with

nanoparticles; phase transitions involving blue phases and TGB phases. From these experimental data, it should be clear that the fact that ASC directly results in the enthalpy as a function of temperature is a unique feature allowing discrimination between (even very weakly) first-order transitions and second-order transitions. Also, for second-order transitions the combination of C_p (the temperature derivative of the enthalpy) with the quantity C introduced in Equation (7) and Figure 4 is a powerful tool to determine the relevant critical exponent α. Other types of liquid crystal phase transition, not discussed here, have also been investigated by ASC, e.g. the smectic A to smectic C transition, the nematic to smectic C, smectic A to hexatic B transition and the nematic-smectic A-smectic C multicritical point (*71–74*).

References

(1) de Gennes, P.G.; Prost, J. *The Physics of Liquid Crystals*; Clarendon: Oxford, 1993.
(2) Vertogen, G.; de Jeu, W.H. *Thermotropic Liquid Crystals, Fundamentals*; Springer-Verlag: Berlin, 1988.
(3) Collings, P.J.; Hird, M. *Introduction to Liquid Crystals: Chemistry and Physics*, Taylor and Francis: London, 1997.
(4) Thoen, J. *Int. J. Mod. Phys.* **B9**, 2157–2218 (1995); In *Liquid Crystals in the Nineties and Beyond*, Kumar, S. Ed.; World Scientific: Singapore, 1995; pp. 19–80.
(5) Thoen, J. In *Physical Properties of Liquid Crystals*, Demus, D.; Goodby, J.; Gray, G.W.; Spiess, H.W. and Vill, V. Eds.; Wiley-VCH: Weinheim, 1997; pp. 208–232.
(6) Garland, C.W. In *Liquid Crystals, Experimental Study of Physical Properties and Phase Transitions*, Kumar, S. Ed.; Cambridge University Press: Cambridge, 2001; pp. 240–294.
(7) Van Roie, B.; Leys, J.; Denolf, K.; Glorieux, C.; Pitsi, G.; Thoen, J. *Phys. Rev.* **2005**, *E72*, 041702(1–8).
(8) Callen, H.B. *Thermodynamics and an Introduction to Thermostatistics*, Wiley: New York, 1985.
(9) Stanley, H.E. *Introduction to Phase Transitions and Critical Phenomena*, Oxford University Press: Oxford, 1971.
(10) Ehrenfest, P. *Proc. R. Acad. Sci. Amsterdam* **1933**, *36*, 153–157.
(11) Nernst, W. *Ann. Phys.* **1911**, *36*, 395–439.
(12) Thoen, J.; Bloemen, E.; Marijnissen, H.; Van Dael, W. In *Proceedings of the 8th Symposium on Thermophysical Properties*, Maryland, 1981; Am. Soc. Mech. Eng: New York, 1982, pp. 422–428.
(13) Thoen, J. In *Phase Transitions in Liquid Crystals*, NATO ASI Ser. B; Martellucci, S. and Chester, A.N., Eds.; Plenum: New York, 1992; pp. 155–174.
(14) Thoen, J. In *Heat Capacities: liquids, solutions, vapours*, Letcher, T. and Wilhelm, E. Eds.; Royal Soc. Chem.: London, 2009; Ch. 13, in press.
(15) Thoen, J.; Bloemen, E.; Van Dael, W. *J. Chem. Phys.* **1978**, *68*, 735–744.
(16) Bloemen, E.; Thoen, J.; Van Dael, W. *J. Chem. Phys.* **1980**, *673*, 4628–4635.
(17) Thoen, J.; Marijnissen, H.; Van Dael, W. *Phys. Rev. A* **1982**, *26*, 2886–2905.
(18) Cordoyiannis, G.; Apreutesei, D.; Mehl, G.H.; Glorieux, C.; Thoen, J. *Phys. Rev.* **2008**, *E78*, 011708(1–5).
(19) Landau, L.D.; Lifshitz, E.M. *Statistical Physics*, Pergamon Press: London, 1959; Ch. 9.
(20) Chaikin P.M.; Lubensky, T.C. *Principles of Condensed Matter Physics*, Cambridge University Press: Cambridge, 1995.
(21) Anisimov, M.A. *Mol. Cryst. Liq. Cryst.* **1988**, *162A*, 1–96.
(22) Detremerie, F. Lic. Thesis, Leuven, 1984.
(23) Thoen, J.; Detremerie, F. (unpublished).
(24) Marijnissen, H.; Thoen, J.; Van Dael, W. *Mol. Cryst. Liq. Cryst.* **1983**, *97*, 149–161.
(25) Cordoyiannis, G.; Kutnjak, Z.; Lahajnar, G.; Glorieux, C.; Thoen, J. *Liquid Crystals* **2009**, *36*, 231–237.
(26) Cordoyiannis, G.; Pinto, L.F.V.; Godinho, M.H.; Glorieux, C.; Thoen, J. *Phase Transitions* **2009**, *82*, 280–289.
(27) Anisimov, M.A. *Mol. Cryst. Liq. Cryst.* **1988**, *162A*, 1–96; and references therein.
(28) Kasting, G.B. Lushington, K.J.; Garland, C.W. *Phys. Rev. B* **1980**, *22*, 321–331.
(29) Chirtoc, I.; Chirtoc, M.; Glorieux, C.; Thoen, J. *Liq. Cryst.* **2004**, *31*, 229–240.
(30) Keyes, P. *Phys. Lett. A* **1978**, *67*, 132–134.
(31) Anisimov, M.A.; Zaprudskii, V.M.; Mamnetskii, V.M.; Sorkin, E.L. *JETP Lett.* **1979**, *30*, 491–494.
(32) Anisimov, M.A.; Gorodekskii, E.E.; Zaprudskii, V.M. *Sov. Phys. Usp.* **1981**, *24*, 57–75.
(33) Garland C.W.; Nounesis, G. *Phys. Rev. E* **1994**, *49*, 2964–2971.
(34) Kobayashi, K. *Phys. Lett. A* **1970**, *31*, 125–126.
(35) McMillan, W.L. *Phys. Rev A* **1970**, *4*, 1238–1246.
(36) de Gennes, P.G. *Mol. Cryst. Liq. Cryst.* **1973**, *21*, 49–76.
(37) de Gennes, P.G. *Sol. St. Commun.* **1972**, *10*, 753–756.
(38) Jamée, P.; Pitsi, G.; Thoen, J. *Phys. Rev. E* **2003**, *67*, 031703(1–9).
(39) Cordoyiannis, G.; Glorieux, C.; Thoen, J. (to be published).
(40) Thoen, J.; Marynissen, H.; Van Dael, W. *Phys. Rev. Lett.* **1984**, *52*, 204–207.
(41) Marijnissen, H.; Thoen, J.; Van Dael, W. *Mol. Cryst. Liq. Cryst.* **1985**, *124*, 195–203.
(42) Garland, C.W.; Kasting, G.B.; Lushington, K.J. *Phys. Rev. Lett.* **1979**, *43*, 1420–1424.
(43) Lubensky, T.C. *J. Phys. C* **1975**, *1*, 151–152.
(44) Benguigui, L. *Liq. Cryst.* **1998**, *25*, 505–515.
(45) Denolf, K.; Van Roie, B.; Glorieux, C.; Thoen, J. *Phys. Rev. Lett.* **2006**, *97*, 107801(1–4).
(46) Denolf, K.; Cordoyiannis, G.; Glorieux, C.; Thoen, J. *Phys. Rev. E* **2007**, *76*, 051702(1–9).
(47) G. Cordoyiannis, L. Kurihara, L. J. Martinez-Miranda, C. Glorieux, and J. Thoen, *Phys. Rev. E* **2009**, *79*, 011702(1–5).
(48) Iannacchione, G.S.; Garland, C.W.; Mang, J.T.; Rieker, T.P. *Phys. Rev. E* **1998**, *47*, 5966–5979.
(49) Clegg, P.S.; Stock, C.; Birgeneau, R.J.; Garland, C.W.; Roshi, A.; Iannacchione, G.S. *Phys. Rev. E* **2003**, *67*, 021703(1–13).
(50) Leheny, R.L.; Park, S.; Birgeneau, R.J.; Gallani, J.-L.; Garland, C.W.; Iannacchione, G.S. *Phys. Rev. E* **2003**, *67*, 011708(1–13).
(51) Iannacchione, G.S.; Park, S.; Garland, C.W.; Birgeneau, R.J.; Leheny, R.L. *Phys. Rev. E* **2003**, *67*, 011709(1–13).

(52) Cruceanu, F.; Liang, D.; Leheny, R.B.; Garland, C.W.; Iannacchione, G.S. *Phys. Rev. E* **2009**, *79*, 011710(1–8).
(53) Garland C.W.; Iannacchione, G.S. *J. Phys. Chem. B*, (in press).
(54) Crooker, P.P. *Liq. Cryst.* **1989**, *5*, 751–775.
(55) Wright D.J.; Mermin, N.D. *Rev. Mod. Phys.* **1989**, *61*, 385–432.
(56) Seideman, T. *Rep. Prog. Phys.* **1990**, *53*, 659–705.
(57) Grebel, H.; Hornreich, R.M.; Shrikman, S. *Phys. Rev. A* **1984**, *30*, 3264–3278.
(58) Thoen, J. *Phys. Rev. A* **1988**, *37*, 1754–1759.
(59) Kutnjak, Z.; Garland, C.W.; Passmore, J.L.; Collings, P.J. *Phys. Rev. Lett.* **1995**, *74*, 4859–4862.
(60) Kutnjak, Z.; Garland, C.W.; Schatz, C.G.; Collings, P.J.; Booth, C.J.; Goodby, J.W. *Phys. Rev. E.* **1996**, *53*, 4955–4963.
(61) Anisimov, M.A.; Agayan, V.A.; Collings, P.J. *Phys. Rev. E* **1998**, *57*, 582–595.
(62) Lubensky, T.C.; Stark, H. *Phys. Rev. E* **1996**, *53*, 714–720.
(63) S. R Renn and T. Lubensky, *Phys. Rev. A* **1988**, *38*, 2132–2147.
(64) Renn, S.R *Phys. Rev. A* **1992**, *45*, 953–976.
(65) Goodby, J.W.; Waugh, M.A.; Stein, S.M.; Chin, E.; Pindak, R.; Patel, J.S. *Nature* **1989**, **337**, 449–452.
(66) Onusseit, H.; Stegemeyer, H. *Z. Naturforsh. Teil A* **1984**, *392*, 658–661.
(67) Nguyen, H-T.; Sallen, C.; Babeau, A.; Galvan, J.M.; Destrade, C. *Mol. Cryst. Liq. Cryst.* **1987**, *154*, 147–154.
(68) Li, M-H.; Nguyen, H-T.; Sigaud, G. *Liq. Cryst.* **1996**, *20*, 361–365.
(69) Jamée, P.; Pitsi, G.; Li, M-H.; Nguyen, H-T.; Sigaud, G.; Thoen, J. *Phys. Rev. A* **2000**, *62*, 3687–3693.
(70) Yang, D.K.; Crooker, P.P. *Phys. Rev. A* **1987**, *35*, 4419–4423.
(71) Thoen, J.; Seynaeve, G. *Mol. Cryst. Liq. Cryst.* **1985**, *127*, 229–256.
(72) Anisimov, M.A.; Voronov, V.P.; Kulkov, A.O.; Kholmurodov, F. *J. Physique* **1985**, *46*, 2137–2143.
(73) Thoen J.; Parret, R. *Liq. Cryst.* **1989**, *2*, 479–488.
(74) Van Roie, B.; Denolf, K.; Pitsi G.; Thoen, J. *Eur. Phys. J. E* **2005**, *16*, 361–364.